ELSEVIER

Progress in Quantum Electronics 35 (2011) 77–108

Progress in Quantum Electronics

www.elsevier.com/locate/pquantelec

Review

Semiconductor infrared up-conversion devices

Y. Yang[a,b], Y.H. Zhang[a,b], W.Z. Shen[a,b,*], H.C. Liu[a,b,*]

[a]*Laboratory of Condensed Matter Spectroscopy and Opto-Electronic Physics, Department of Physics, Shanghai Jiao Tong University, Shanghai 200240, China*

[b]*Key Laboratory of Artificial Structures and Quantum Control (Ministry of Education), Department of Physics, Shanghai Jiao Tong University, Shanghai 200240, China*

Available online 27 May 2011

Abstract

Various infrared up-conversion techniques have been developed, driven by applications including lasing, laser cooling, and infrared imaging. In this review article, we first present a brief overview of existing up-conversion techniques and then discuss in detail one particular approach. Among all types of up-conversion techniques, an integrated semiconductor photodetector-light-emitting diode (PD-LED) up-conversion device is the most promising one for infrared imaging applications. By now, PD-LED devices relying on various mechanisms, using different materials and structures, aiming at different wavelength regions, have been developed, and pixelless infrared imaging prototype devices have been demonstrated. We report the progress of semiconductor PD-LED up-conversion devices, and point out directions for future improvement.

Keywords: Infrared; Up-conversion; Imaging; Semiconductor; Photodetector; Light-emitting diode

Contents

*Corresponding authors at: Department of Physics, Shanghai Jiao Tong University, Shanghai 200240, China.
E-mail addresses: wzshen@sjtu.edu.cn (W.Z. Shen), h.c.liu@sjtu.edu.cn (H.C. Liu).

0079-6727/$ - see front matter
doi:10.1016/j.pquantelec.2011.05.001

1. Introduction

The process of photon up-conversion is to convert photons from low to high frequencies. Of particular interest is from infrared to near-infrared (NIR) or visible. So far, a variety of applications have been exploited based on infrared up-conversion, including lasing [1–4], three-dimensional (3D) display [5–7], up-conversion enhanced solar cells [8–10], laser cooling [11–14], up-conversion based weak infrared photon detection [15–19], and infrared imaging [20–22]. In this review article, we focus on the infrared up-conversion devices for the purpose of infrared imaging.

For imaging in the visible and NIR region below 1 μm in wavelength, Si charge coupled devices (CCDs), and lately Si complementary metal–oxide–semiconductor (CMOS) arrays, with high performance and low price are widely available. Si CCD was invented by W.S. Boyle and G.E. Smith at Bell Labs in 1969. Since 1971, CCDs found applications in visible and NIR imaging. In 1974, linear CCDs with 500 elements and two-dimensional (2D) devices with 100×100 pixels were developed. By now, high performance 2D CCDs and CMOSs with up to millions of pixels are manufactured in large scales. Using intrinsic interband transition, the wavelength range covered by Si CCDs and CMOSs is from about 200 nm to about 1 μm. Standard commercial CCDs and CMOSs are produced in mass quantities; used in our daily lives. For example, most cell phones sold in the market are equipped with a CCD or CMOS array with several millions of pixels.

In contrast, infrared imaging for wavelengths longer than 1 μm is lagging far behind. Infrared imaging systems are divided into two categories, scanning and starring [23]. In a scanning system, infrared images are taken using a single-element photodetector (PD) or a linear PD array in combination with a mechanical scanner, while a starring array is a 2D PD matrix with thousands or millions of discrete pixels. The starring infrared imager is superior to the scanning system in terms of sensitivity and compactness. 2D focal planar array (FPA) has become the current industry standard for infrared imaging. Various infrared imaging devices have been developed, depending on the wavelength. In the short wavelength infrared region less than about 2 μm, the mainstream is InGaAs FPAs on InP substrate. For the middle and long wavelength infrared region, HgCdTe, InSb, and quantum well infrared photodetector (QWIP) FPAs compete with one another. So far, infrared FPAs with hundreds of thousands of pixels or more, pixel sizes of several tens of μms, and noise equivalent temperature difference (NETD) of several mK have been developed [23–27]. Table 1 illustrates the comparison of Si CCD/CMOS with some of the best developed infrared imaging devices.

As schematically depicted in Fig. 1, a FPA is composed of a matrix of PD units and a read-out integrated circuit (ROIC). The PD matrix and ROIC are generally fabricated on different materials, and then interconnected with each other by Indium bump-bonding technology, a time-consuming and costly process [23]. Although researchers have tried to develop monolithic FPAs using narrow-gap semiconductors, so far FPAs bump-bonded with Si ROICs remain the only practical choice, consequently the cost stays high: A 512×480 InGaAs FPA costs about 10 thousands dollars, and an InSb or HgCdTe FPA costs even more. FPAs were initially driven by military applications such as missile seeking/guidance and night vision, which are less cost sensitive than other applications [28,29]. More recently, FPAs have been expanded to civil applications. For example,

Table 1
Comparison of Si CCD/CMOS with some of the best developed infrared imaging devices.

	Wavelength range (μm)	Detectivity (cm $Hz^{1/2}$/W)	Typical format	Typical pixel size (μm)	Operation temperature	Price range (dollars)
Si CCD/CMOS	0.2–1	$\sim 10^{14}$	2048×2048	~10	Room temperature	Less than 100
InGaAs FPA	1–2	$\sim 10^{11}$	640×512	~20	Thermoelectric temperature	More than 10,000
InSb FPA	1–5	$\sim 10^{10}$	640×512	~20	Liquid nitrogen temperature	More than 10,000
HgCdTe FPA	3–14	$\sim 10^{10}$	640×512	~20	Liquid nitrogen temperature	More than 10,000
QWIP FPA	3–20	$\sim 10^{10}$	640×512	~20	Liquid nitrogen temperature	More than 10,000

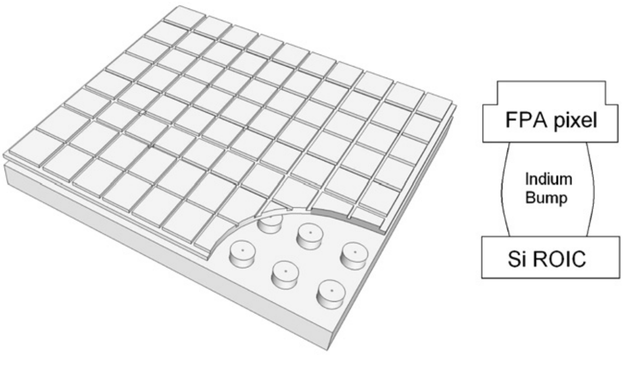

Fig. 1. A schematic of a 2D FPA, and the simplified structure of a FPA pixel connected with Si ROIC by Indium bump.

mid-infrared (MIR) FPAs are used to find flaws in architectures [30], while NIR FPAs are employed in medical examination to detect breast cancer [31,32]. Yet, the civil market of FPAs remains quite small, mainly limited by the high price. Therefore, there is a need for low-cost infrared imaging device technologies.

One alternative approach of infrared imaging is to up-convert the infrared photons to higher frequencies and then detect them with Si CCDs. Fig. 2 depicts a schematic of infrared up-conversion imaging system. Incident infrared photons beyond 1 μm are ‘‘transferred’’ by an up-conversion device to visible or NIR photons below 1 μm, which are then collected with a Si imaging device. In some cases, there is no need for the up-conversion device to have discrete pixels, leading to a ‘‘pixelless’’ imaging device. Compared with FPAs, pixelless imaging based on up-conversion can be a much cheaper way for infrared imaging because no pixels need to be patterned on the up-conversion device and the expensive Indium bumping step is avoided.

Until now, several up-conversion techniques have been developed, including thermally excited up-conversion [11–14], parametric up-conversion [15–19,33–35], rare-earth up-conversion [1–10], Auger process [36–41], two-step two-photon absorption (TS-TPA) up-conversion [42–49], and PD-light-emitting diode (LED) up-conversion [21,22,50–85]. These techniques rely on different mechanisms, with their own advantages and drawbacks. In Section 2, we briefly introduce and compare them. Among all up-conversion techniques, PD-LED up-conversion devices are the most promising for the purpose of up-conversion imaging.

The main section of this review, Section 3, is devoted to PD-LED infrared up-conversion devices, especially NIR PD-LED up-conversion devices. In Section 3.1, we report the progress on NIR PD-LED up-conversion based on InP and GaAs substrates, the most commonly used NIR material systems. Section 3.2 presents a brief introduction to wafer fusion, an advanced fabrication technique for optoelectronic devices, which have been used to fabricate NIR up-conversion devices with high efficiencies. Section 3.3 discusses the LED internal and external quantum efficiencies, which are crucial to the performance of up-conversion devices. Section 3.4 is dedicated to the introduction of special types of NIR up-conversion devices, including (1) the phototransistor-LED NIR up-conversion devices, which have the potential to achieve high up-conversion efficiencies beyond unity, (2) the two photon passive up-conversion device, which does not need bias voltages, (3) the internal photoemission NIR up-conversion devices, and (4) the organic PD-LED up-converters. In Section 3.5, we review up-conversion infrared imaging.

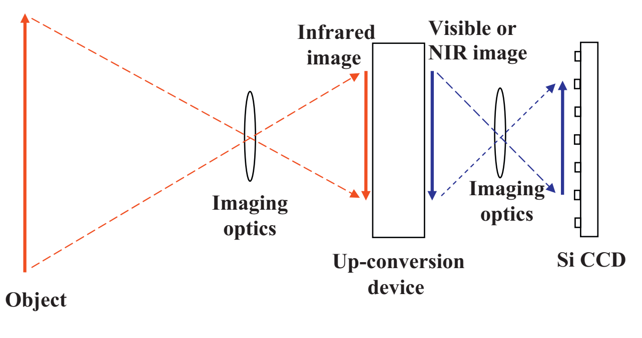

Fig. 2. A schematic of infrared up-conversion imaging.

2. Up-conversion techniques

2.1. Thermally excited up-conversion

To satisfy energy conservation law, an extra energy is needed to up-convert infrared photons to higher frequencies. In thermally excited up-conversion, incident photons interact with the host material and obtain extra energies from the phonons or other excitations. At the same time, the host material losses heat, resulting in cooling. Thermally excited up-conversion has been employed for characterization of materials, and laser cooling of atoms, molecules, gases and condensed state materials. Laser cooling was first experimentally demonstrated in 1968 by Kushida and Geusic [11] using YAG doped with Nd^{3+}. The pump source was a 1.064 μm laser, and the emitted light had a wavelength of 0.946 μm. The magnitude of laser cooling was determined to be about 0.6 K, under 100 W laser pump and atmosphere pressure condition.

Later, laser cooling of gas-phase atoms was demonstrated, and Bose–Einstein condensation of the atomic ensemble was observed [12]. Thereafter, Mungan et al. [13] demonstrated laser cooling of a solid by 16 K starting from room temperature (RT) using thermally excited up-conversion. In 2009, Seletskiy et al. [14] reported laser cooling of ytterbium-doped $LiYF_4$ crystal to a temperature of 155 K starting from RT, with a cooling power of 90 mW. However, it should be noted that the excess energy between the emitted and excitation photons can be only a few k_BT in thermally excited up-conversion. At RT, it is several tens meV.

2.2. Parametric up-conversion

For other types of up-conversions (parametric up-conversion, rare-earth up-conversion, Auger up-conversion, and TS-TPA), the basic idea is to convert two or several low energy photons to one with a higher energy. In a nonlinear optical media, the dielectric polarization P responds nonlinearly to electric field E. When two groups of photons with frequencies of v_1 and v_2 travel through a nonlinear media simultaneously, photons with frequencies of v_1+v_2 can be generated. This optical process is called parametric up-conversion (or sum frequency generation), during which the energy conservation law is satisfied. Parametric up-conversion has been used to detect both infrared [15,20] and terahertz radiation [34].

Fig. 3 schematically shows an example of parametric up-conversion imaging [20]. The 10.6 μm laser diffused from the scatter plate carried the infrared information to be detected. The 0.693 μm laser worked as the local pump source. The two lasers were incident into a mixing medium, proustite (Ag_3AsS_3) crystal, generating the output photons at wavelength 0.6516 μm. It was a complex system with many optical components. A powerful laser was needed as the pump source. To screen the 0.693 μm laser from the 0.6516 μm output signal, polarizer and filters were placed between the mixer and imaging optics. To have an effective up-conversion, one key point is to satisfy the condition of phase-matching (momentum conservation), which is difficult to achieve.

More recently, periodically poled lithium niobate (PPLN) have been used as the mixer, and high efficiency parametric up-conversions were demonstrated. In 2004, Albota and Wong [15] reported efficient single-photon counting at 1.55 μm using parametric up-conversion with PPLN. The existing way of single photon detection around 1.55 μm is to use InGaAs APDs. InGaAs APDs can only work under pulsed mode at low frequencies,

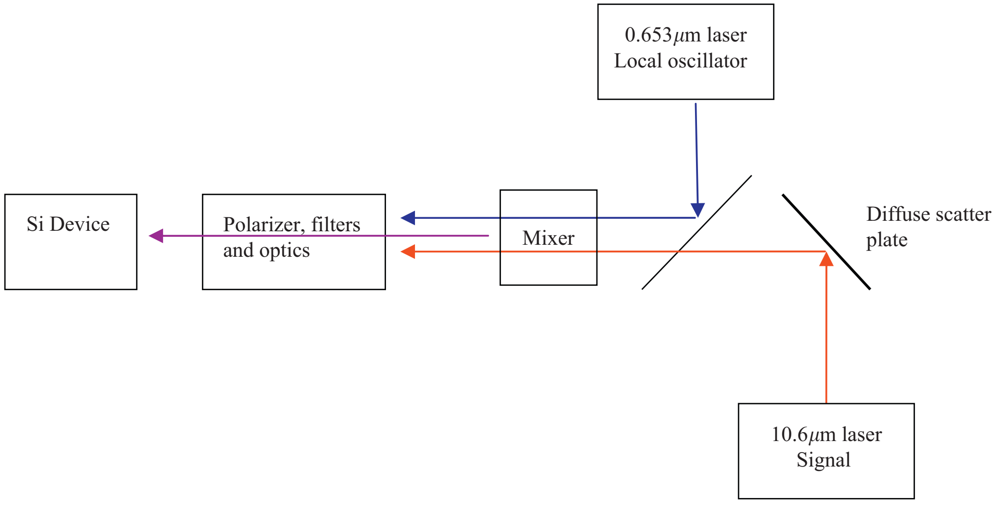

Fig. 3. Experimental setup for parametric up-conversion imaging.

and the efficiency is low (less than 20%). In comparison, Si APD single-photon counting modules have high quantum efficiencies (about 70%), low dark count rates (<100/s), and can work in continuous mode. In the experiment, 1.55 μm photons were mixed with a strong 1.064 μm pump in PPLN to produce 0.631 μm visible light. The up-conversion efficiency reached 90%.

2.3. Rare-earth up-conversion

The best developed up-conversion approach is rare-earth up-conversion. Rare-earth ions such as Er^{3+}, Tm^{3+}, Ho^{3+}, Nd^{3+}, and Pr^{3+} have metastable intermediate excitation levels. They can absorb two or several photons and arrive at high energy levels. The ions will then return to lower energy states after single or multiple-photon relaxation, emitting photons with higher energy than the absorbed ones. Fig. 4 shows the energy level diagram of Er^{3+} to explain rare-earth doped system up-conversion mechanism. As indicated, after absorbing two 797 nm photons, the ion is excited from energy level $^4I_{15/2}$ to higher energy level $^2H_{11/2}$, and relaxes to the lower level producing visible light at about 540 nm [1].

RT rare-earth up-conversion devices with high efficiencies and output powers have been developed now. The response wavelength has covered the NIR and MIR region, and the output wavelength has covered the NIR and whole visible wavelength region. Rare-earth ions can be easily incorporated in various hosts, including crystals, glass, and optical fiber to produce visible laser, pumped by high power infrared lasers. Rare-earth up-conversion technique has also been explored for applications of 3D display, and solar cells.

Like rare-earth ions, some transition metals ions have been doped in host materials to realize photon up-conversion [3]. Transition metals ions used for up-conversion include Ti^{2+}, Ni^{2+}, Mo^{3+}, Re^{4+}, Os^{4+}, Mn^{2+}, and Cr^{3+}. It was found that high performance up-conversion devices can be fabricated by incorporating rare-earth ions and transition metal ions simultaneously [3]. The transition metal ions will interact with rare-earth ions, and make them more sensitive for infrared up-conversion.

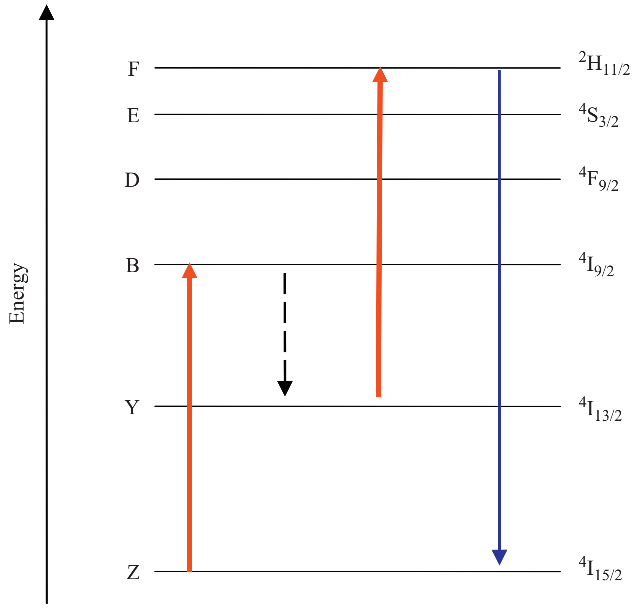

Fig. 4. A schematic of rare-earth up-conversion.

2.4. *Auger up-conversion*

Auger process is a three-particle process, involving two electrons and one hole, or two holes and one electron. During Auger recombination between an electron and a hole, the released energy is transferred to the third particle (electron or hole), bringing it to higher energy levels. Interestingly, photon up-conversion based on this well-known non-radiative process has been demonstrated.

Photon up-conversion based on Auger process was observed from the spin–orbit split-off band in bulk GaSb material [36], and later demonstrated in doped quantum wells [37]. In 1994, Seidel et al. [38] demonstrated high efficiency Auger up-conversion in InP/AlInAs Type-II heterostructures. Under the illumination of 1.325 eV laser, a sharp 1.41 eV emission was observed. At an excitation density of the order of 10 kW/cm^2, the up-conversion efficiency reached nearly 50%. It is worth noting that the Auger up-conversions can also happen at low excitation intensities of 0.1–1 W/cm^2, much lower than the intensity required for the parametric up-conversion, and the rare-earth up-conversion.

In 1995, Driessen et al. [39] reported photon up-conversion at GaAs–GaInP$_2$ type-I interface, and attributed it to Auger process. The excitation source was 1.5 eV laser and the up-converted signal peaked at about 1.9 eV, corresponding to an energy increase of 400 meV. Fig. 5 depicts a schematic of the Auger up-conversion at the GaAs–GaInP$_2$ Type-II heterostructures. First, two electrons are excited from the valence band to conductance band by incident IR photons at the interface. One of the excited electrons recombines with a hole there through non-radiative Auger process. The released energy is transferred to another electron, and excites it to higher energy level. It will then radiatively recombine with a hole if the final stage is sufficiently metastable, producing a photon with higher energy than the incident light. Later, they reported an up-conversion of 700 meV at GaAs–GaInP$_2$ type-I interface, at operation temperatures ranged from 8 to 200 K [40].

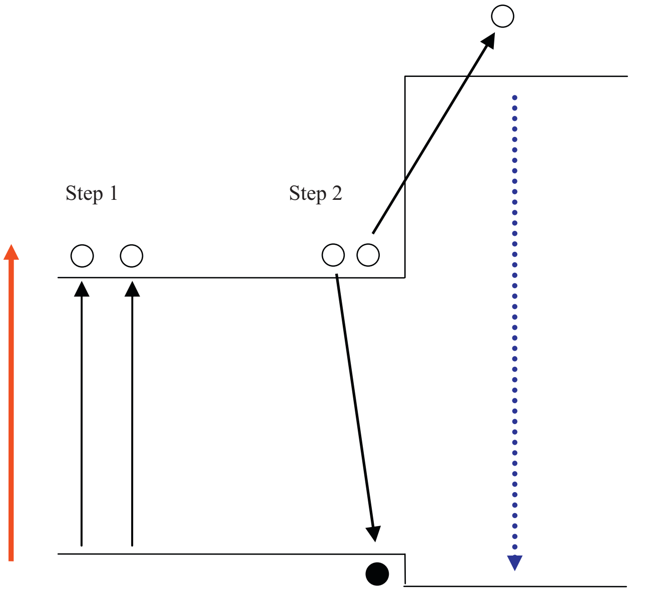

Fig. 5. A schematic of Auger up-conversion.

2.5. Two-step two-photon absorption up-conversion

TS-TPA up-conversion has been demonstrated with structures having either type-I or type-II band alignments. In 1993, Tomita et al. [42] observed TS-TPA up-conversion in asymmetrical GaAs/AlGaAs double quantum well structures (type I). The same effect was then observed at CdTe/(Cd,Mg)Te multiple quantum well structures [43]. In 1996, Su et al. [44] studied the up-conversion phenomenon with a GaAs/(ordered)$GaInP_2$ heterostructure. Under the excitation of an 808 nm laser, output light peaked at 653 nm was observed. The excitation power density was estimated to be no larger than 300 W/cm^2, which is not high enough for nonlinear optical process to occur.

In order to explain the experimental results, Su et al. [44] proposed the models of up-conversion at two different types of heterostructure interfaces. Fig. 6(a) schematically illustrates the two-step process at the interface of type-I heterojunction with large barrier heights. With the absorption of the first incident photon, an electron–hole pair in the quantum well was created. With the absorption of the second photon, the electron is excited above the quantum barrier, which would then recombine with a hole and radiate a photon with higher frequency. On the other hand, a hole instead of an electron is excited by the second absorbed photon at the heterojunction with small barrier heights [Fig. 6(b)].

2.6. PD-LED up-conversion

In 1967, Kruse et al. [50] reported the earliest realization of PD-LED NIR up-conversion device. As depicted in Fig. 7(a), it was an *n–p–n* structure with a Ge/GaAs heterojunction as the PD, and a GaAs homojunction as the LED. The up-conversion spectrum of this NIR up-conversion device is displayed in Fig. 7(b) [50]. It had a peak

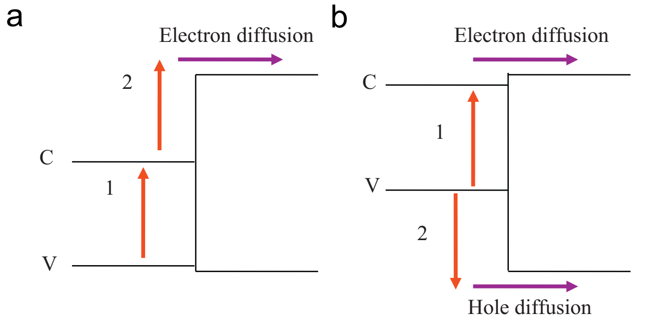

Fig. 6. TS-TPA process at type-I heterojunctions with (a) high and (b) low barrier heights.

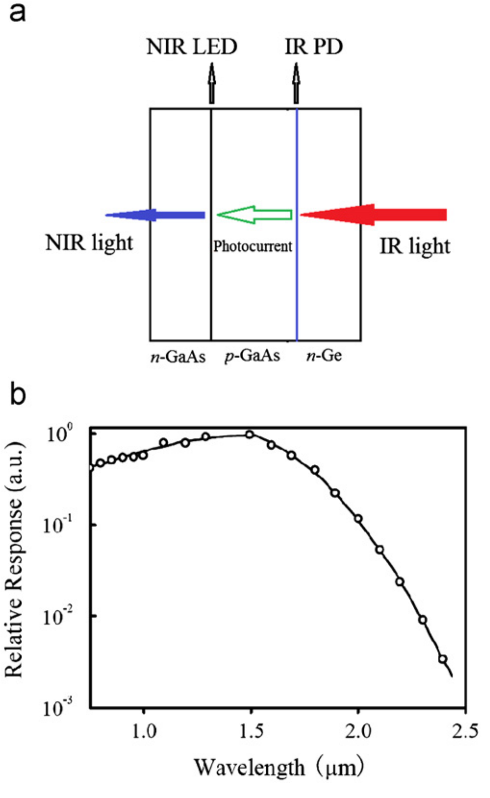

Fig. 7. (a) Solid state infrared converter employing Ge-GaAs heterojunction PD and GaAs homojunction LED and (b) the up-conversion spectrum (from Ref. [50]).

response at 1.5 μm and a cutoff wavelength of about 1.7 μm, typical for Ge material, and the wavelength of emitted photons was 0.9 μm. It suffered from a poor up-conversion efficiency of 2.8×10^{-5} W/W, since both the Ge/GaAs heterojunction PD and the GaAs homojunction LED had low efficiencies. Similar to this prototype, all PD-LED up-conversion devices are typically composed of two major parts, a PD and a LED.

Incident infrared photons are absorbed by the PD, resulting in a photocurrent that drives the LED to emit photons with shorter wavelengths. In most PD-LED devices, the extra energy for up-conversion comes from the applied electric field.

Later that year, an InSb/GaAsP up-conversion device was reported. The device used an InSb photodiode to detect 5.3 μm infrared photons and a GaAsP LED to produce photons with wavelengths between 0.6 and 0.7 μm [51]. To get high efficiency, tunable contrast and sensitivity, the device adopted a capacitor–detector–emitter structure. The photocurrent induced charges were integrated and stored by the capacitor, and then delivered to the LED in high-current pulses. The device worked only in pulsed mode, and the up-conversion quantum efficiency was estimated to be 10^{-4}, mainly limited by the LED quantum efficiency. In 1974, a GaAs/AlGaAs NIR up-conversion device with up-conversion efficiency of 1.5% was reported [52]. The cut-off response wavelength of the up-conversion device was 875 nm, and the output emission peaked at 785 nm. Since then, III–V compound semiconductors became the dominant material system for infrared up-conversion.

Research activities continue with investigating PD-LED up-conversion devices by employing novel structures, new materials, and alternative mechanisms. In 1981, Beneking et al. [53] reported a GaAs/AlGaAs NIR up-conversion device with power amplification. Combining a phototransistor and a LED, 820 nm photons were up-converted to 775 and 680 nm. Very high up-conversion efficiencies larger than unity were achieved. In 1991 [55], an organic up-conversion device from red to green was invented, combining an organic LED with a photoresponsive amorphous Si carbide. In 2000, 1.55 μm to 0.87 μm NIR up-conversion device was fabricated by growing an InGaAs/InP PD and an InAsP/InP LED on InP substrate [61]. In 2003, wafer fusion technology was used to fabricate NIR up-conversion devices with high efficiency [65,69]. For NIR up-conversion below 3 μm, a narrow bandgap PD is normally used, but NIR up-conversion devices based on internal photoemission are also worth-noting [62,67,78]. Besides, two-photon NIR up-conversion device that did not need to be biased was reported [86].

In addition to the NIR up-conversion, MIR and far-infrared (FIR) up-conversion devices have been developed. Since 1995, MIR up-conversion devices have been fabricated by epitaxially growing a QWIP with a LED on top [21,22,57–60,64,66,70,74–76]. It has been revealed that an optimized QWIP-LED can have comparable performance to QWIPs alone [76]. For a summary on QWIP-LED MIR up-conversion and pixelless up-conversion imaging, we refer to Ref. [76]. In addition to QWIPs, other PDs such as InSb MIR photodiode [73] and homojunction interfacial work-function internal photoemission FIR PDs [79,83] are investigated for infrared up-conversion.

Among all types of up-conversion techniques, PD-LED up-conversion is the most promising for the purpose of infrared up-conversion imaging, due to the unique characteristics of simplicity and compactness, low cost, wide response range, good flexibility, and high up-conversion efficiency. Table 2 compares the features of all types of up-conversion techniques. As can be seen, PD-LED up-conversion distinguishes itself with the listed characteristics:

1. PD-LED up-conversion devices can work at very low excitation density appropriate for imaging such as in the thermal range of a few mW/cm^2. In contrast, other up-conversion techniques, including the parametric up-conversion and the rare-earth up-conversion need an excitation density threshold in the kW/cm^2 range.

Table 2
Comparison of different up-conversion techniques.

	Excitation density	Operation temperature	Efficiency	Compactness	Response spectrum	Application
PD-LED up-conversion	No threshold	RT or liquid nitrogen temperature	High (can be higher than unity)	Compact	Wide	Infrared imaging
Thermally excited up-conversion	No threshold	RT	Low	Compact	Wide	Laser cooling
Parametric up-conversion	High threshold ($\sim$kW/cm^2)	RT	High (up to unity at high pump power)	Not compact	Narrow	Lasing, single-photon detection, infrared imaging
Rare-earth up-conversion	High threshold ($\sim$kW/cm^2)	RT	High (several tens percents)	Compact	Narrow	Lasing, 3D display, solar cells
Auger process	No threshold	4.2–200 K	High (up to 50% at high excitation density)	Compact	Wide	Potentially infrared imaging
TS-TPA up-conversion	Moderate threshold ($\sim$1–100 W/cm^2)	2–50 K	Low	Compact	Wide	Potentially infrared imaging

2. PD-LED up-conversion devices operate at easily reachable temperatures, i.e., a NIR up-conversion device normally works at RT, and a MIR up-conversion device works at 77 K or higher temperature. Where else, some other up-conversion devices such as TS-TPA work at low operation temperatures of several K.
3. PD-LED up-conversion devices are excellent in terms of up-conversion quantum efficiency. As will be shown, quantum efficiencies of several percent W/W have been achieved for devices without amplification structures, and phototransistor-LED up-conversion devices can have efficiencies higher than unity.
4. PD-LED up-conversion devices are compact and hence the resulting imaging systems can be simple. Pumping lasers, which are usually necessary in other up-conversion techniques, are not required.
5. Another advantage of PD-LED up-conversion devices is that they generally have broad band response, while other up-conversion techniques such as the parametric up-conversion can only convert photons at one or several specific frequencies. Objects normally emit photons covering a wide wavelength range. Thus the majority of the infrared photons will be wasted by using narrow band up-conversion techniques.

In addition, PD-LED up-conversion devices normally have a linear response to the excitation power density. That is, the up-converted light density is proportional to the excitation power density. Meanwhile, most other up-conversion techniques respond super-linearly to the power density. PD-LED up-conversion devices are grown and fabricated with standard semiconductor techniques, including molecular beam epitaxy (MBE), metal organic chemical vapor deposition (MOCVD), lithography, etching, and metal deposition. Therefore, they have the potential to be manufactured at large scale, with good uniformity and low cost.

3. NIR up-conversion devices

3.1. InP- and GaAs-based NIR up-converters

A NIR PD-LED up-converter is composed of a LED and a NIR PD, which can be a narrow bandgap PD or an internal photoemission PD. NIR PDs using interband transition of narrow bandgap semiconductor materials are much more efficient than their counterparts. In the NIR region, InGaAs is the best developed among all III–V compounds. InGaAs PDs now routinely reach responsivity higher than 1 A/W. Besides, they work at RT.

Since 2000, NIR up-conversion devices with InGaAs PD on InP substrate have been fabricated [61,65,69]. Fig. 8(a) shows the structure of the first InP-based NIR up-conversion device, which is a back-to-back *p–i–n* PD and LED, with a common *p*-region in the middle [61]. The active region of the PD is 20 repeats of $In_{0.53}Ga_{0.47}As/InP$, and the LED active region is a 57 nm $InAs_{0.1}P_{0.9}$ layer. During operation, the *p–i–n* photodiode is reverse biased and the LED is forward biased. As shown in Fig. 8(b) [61], the up-converter has a typical InGaAs spectral response in the NIR region, with a cutoff wavelength of 1.6 μm. The dip at 1.4 μm is due to the CO_2 absorption, the shoulder at 1 μm corresponds to the $InAs_{0.1}P_{0.9}$ bandgap absorption, while the peak at 0.9 μm is resulted from the InP absorption. Incoming 1.6 μm laser was absorbed by the *p–i–n* PD, inducing a LED

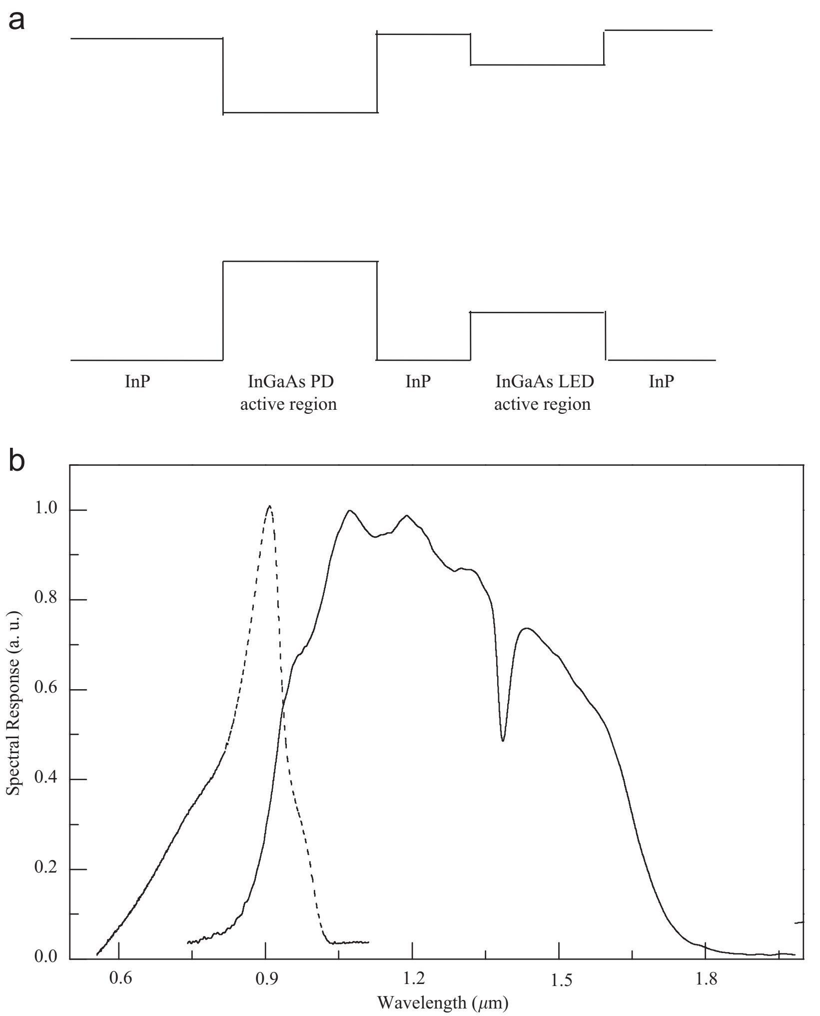

Fig. 8. (a) InP-based NIR PD-LED up-conversion device structure and (b) RT spectral response (from Ref. [61]).

emission at 1 μm which was detected by Si detector. The InGaAs NIR PD has a high responsivity of 2 A/W, implying nearly 100% high-absorption efficiency and photocurrent gain higher than unity. In two other papers [65,69], we fabricated NIR PD-LED up-converters by integrating InGaAs PDs and GaAs-based LEDs. In both cases, the PDs have a responsivity of about 1 A/W.

Except for InGaAs PDs, NIR PDs based on GaAs material have been employed for NIR up-converters. Optoelectronic devices on GaAs substrates are attractive because of the good material uniformity, mature technology, and low cost. The RT bandgap of bulk GaAs material is 1.42 eV, corresponding to a wavelength of 0.87 μm. InGaAs and GaAsSb have narrower bandgaps and can response to longer wavelength, but their lattice constants are larger than GaAs. Fortunately, both the lattice constant and bandgap can be by reduced by doping a small amount of nitrogen into InGaAs or GaAsSb. By now, GaInNAs/GaAs and GaNAsSb/GaAs NIR PDs lattice-matched to GaAs have been fabricated [87–89]. GaAs-based NIR PDs are now able to cover wavelength up to 1.6 μm, with responsivities comparable to InGaAs PDs. An advantage of GaInNAs/GaAs and GaNAsSb/GaAs PDs is that they can be epitaxially grown with GaAs, to realize full-GaAs-based up-converters. With a GaNAsSb/GaAs NIR up-conversion device lattice matched to GaAs substrate, NIR photons below 1.6 μm were up-converted to 0.87 μm, and a high up-conversion efficiency of 0.048 W/W was achieved [85].

3.2. *Wafer fusion*

The bandgap difference between InGaP active region and InP substrate of InP-based LEDs is not large enough to confine the carriers effectively, so carriers easily escape the LED active region. As a result, InGaP/InP LED has low internal quantum efficiencies (less than $<1\%$), and so does the full InP-based up-converter [61]. To improve the LED efficiency, we need to increase the bandgap difference between the active region and the carrier confining layers. A simple way is to increase the As fraction in the active region of the GaAs/AlGaAs LED. However, this would lead to an increasing strain and consequently a substantial degradation of the device performance, when the As fraction exceeds 20% [61]. Higher As fraction will also lead to a longer wavelength emission, where Si devices do not work well.

Compared with InP-based LEDs, GaAs/AlGaAs LEDs are capable of higher efficiencies. Therefore, a straightforward way for increasing up-conversion efficiency is to substitute InP/InGaAs LEDs with GaAs/AlGaAs LEDs. However, there is a large lattice constant difference between GaAs and InP material systems, making it difficult to grow InGaAs/InP PD with GaAs/AlGaAs LED through direct epitaxial growth. Fortunately, this problem could be solved by wafer fusion, an advanced processing technology used for integrating heterogeneous semiconductor materials regardless of their lattice mismatch [90]. It gives a new degree of freedom for the design and fabrication of semiconductor optoelectronic devices. The main advantage of wafer fusion is that the defects, mismatch and interface stress affect no more than several atomic layers at the interface, and the original characteristics of each layer are kept. The wafer fused interface has little optical loss, good thermal and electronic properties.

Wafer fusion consists of several steps including pre-processing of wafer surface, pre-fusion, and thermal treatment [90]. Before fusion, the layers to be fused will go through a few steps including polishing, cleaning, and deoxidation to obtain flat and clean surfaces. The materials are usually polished by chemical methods. After that the surfaces are typically ultrasonically cleaned in acetone, methanol/isopropyl ketone solution to remove dust, organic contaminations and metal impurities, and then cleaned by distilled water and HF solution to remove the intrinsic oxide layer. The clean layers are pressured together to facilitate pre-fusion, due to three types of interactions, Van Der Waals attraction, electrostatic interaction, and capillary force. Afterward, the pre-fused device will be annealed in H_2 or N_2 to obtain a stronger bonding. Annealing reorganizes the structure of fusion interface by helping the atoms and molecules around the vacancies to diffuse, and therefore decreases the density of the vacancies. Fig. 9 shows a transmission electron microscopy (TEM) image of a fused interface between a GaAs layer and an InP layer. Defects and dislocations exist only at the fusion interface confined to a few nanometers thick region.

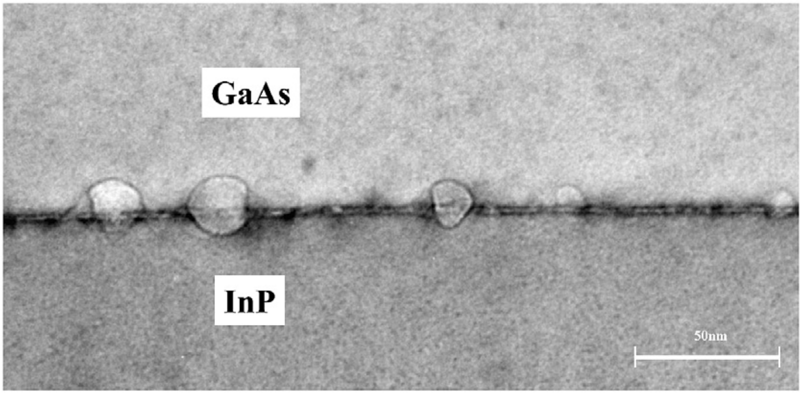

Fig. 9. TEM image of a fusion interface between a GaAs layer and an InP layer.

Wafer fusion has been employed to fabricate a NIR up-converter by integrating a GaAs/AlGaAs LED and an $In_{0.53}Ga_{0.47}As/InP$ *p–i–n* PD [65]. The GaAs/AlGaAs LED structure was grown by MBE on an *n*-type GaAs substrate, with the *p*-contact layer on top. A 400 nm-thick GaAs active region was used, which was confined by *p*- and *n*-type AlGaAs layers. The $In_{0.53}Ga_{0.47}As/InP$ *p–i–n* PD was grown by MOCVD on an *n*-type InP substrate, with the *p*-contact layer on top. The *p*-contact layers of the PD and LED was wafer fused together to form a *p–i–n* LED structure. The GaAs substrate of the LED was then chemically removed, and then the device mesas and contacts are fabricated. The device successfully up-converted 1472 nm incident laser radiation to 872 nm LED emission. Fig. 10 shows the device structure and experimental results [65]. The PD responsivity remains about 0.8 A/W in applied bias range between 0.5 and 5.0 V. The LED external efficiency increases with increased applied bias. At 4 V bias, the measured LED external efficiency is 0.0064 W/A, corresponding to an internal quantum efficiency of around 27%. Later, wafer fusion was used to integrate an InGaAs/InP photodiode with an optimized GaAs/AlGaAs LED with near 100% internal efficiency, where high up-conversion efficiency of 0.018 W/W was obtained [69].

3.3. LED efficiency

On the light-emitting side, the overall LED efficiency is the product of the internal efficiency and photon escape probability. The former is the probability of a photon produced for each electron–hole pair injected into the LED active region, while the later is photon escape probability from the LED surface.

3.3.1. LED internal efficiency

LED internal efficiency is determined by three major electron–hole recombination mechanisms within the LED active layer: the Shockley–Hall–Reed (SHR) recombination, the Auger recombination, and bimolecular or spontaneous radiative recombination. For the purpose of high LED quantum efficiencies, high radiative recombination is desired. During SHR recombination, the excess energies are dissipated as phonons, and the momentum differences are absorbed by impurities within the bandgap. SHR recombination is normally

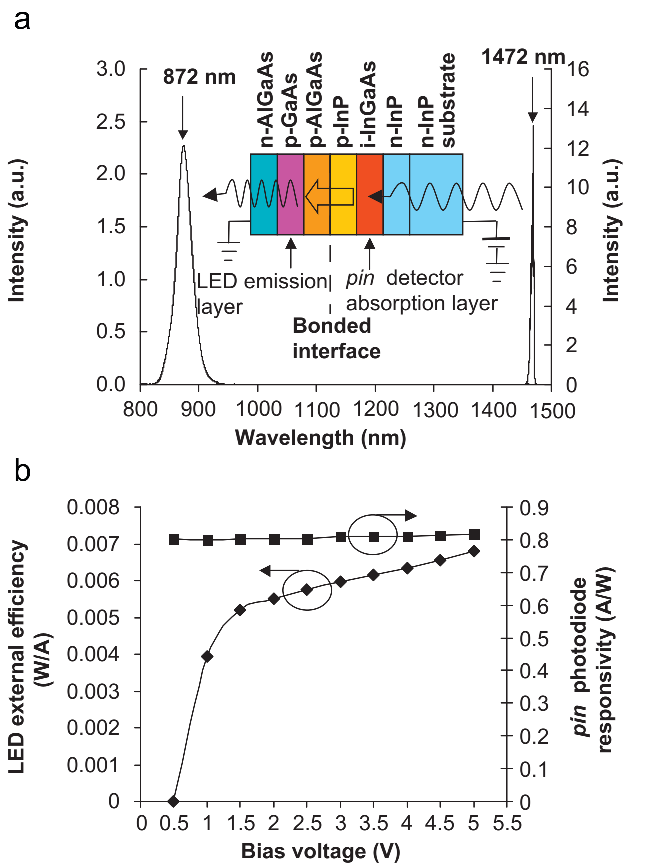

Fig. 10. 1.5–0.87 μm PD-LED up-conversion device fabricated by wafer fusion (a) the device structure and (b) the bias dependant performances [65].

the dominant process in indirect bandgap materials. It is also prominent in direct bandgap materials at very low injection levels, and with low doping densities. On the other hand, non-radiative Auger process is only significant at high injection levels.

The operating current density (typically between 0.001 and 1.0 A/cm^2) of up-converters is much smaller than that of most conventional LED applications. Thus the parameters of the LED structures need to be optimized for this particular purpose. In 2004, Ban et al. optimized *p*-doping concentrations in the GaAs/AlGaAs LED active region for room temperature up-conversion device. Fig. 11(a) shows the dependence of LED quantum efficiency on LED active region doping concentration, for room temperature operation and low injection current [69].

With a low doping concentration and at a low injection level, the SHR non-radiative recombination plays an important role, and the current injection was not sufficient. As a result, the LED efficiency was low. At high doping concentration (3×10^{18} cm^{-3} or more), the Auger non-radiative recombination starts to play an important role, resulting a decreased LED efficiency. The experimental and theoretical results revealed that the radiative recombination dominates only in the moderate doping concentration range from

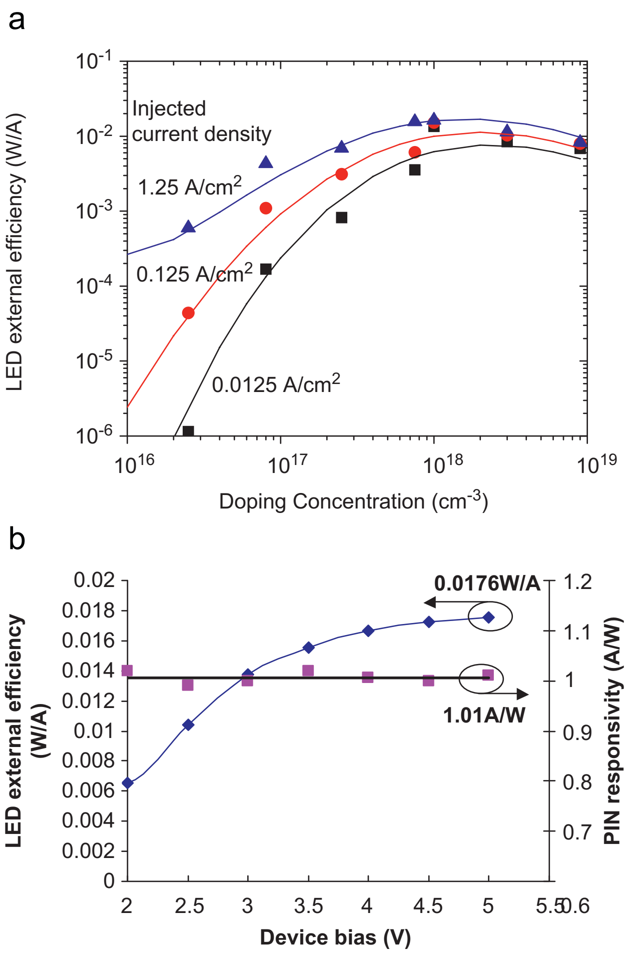

Fig. 11. (a) The dependence of LED external efficiency on doping concentration for different injection current densities and (b) the performance of a PD-LED up-conversion device with an optimized LED (from Ref. [69]).

5.0×10^{17} to 2.0×10^{18} cm^{-3} for low current levels (1.0 A/cm^2 or smaller). The optimal *p*-doping concentration for the LED active region was found to be 1×10^{18} cm^{-3}, and a near 100% internal quantum efficiency was achieved at RT [69].

The LED with the optimal design was then wafer fused with an InGaAs/InP PD to get a NIR up-conversion device. Fig. 11(b) shows the performance of the up-conversion device. The PD has a responsivity of about 1.0 A/W, corresponding to an absorption efficiency of 86%. The LED has an efficiency of 0.0176 W/A at 5 V bias, corresponding to an internal efficiency of 87%. Therefore, the total internal up-conversion quantum efficiency of the integrated device reached 76% at 5 V bias.

3.3.2. LED external efficiency

Despite of high internal efficiency achieved, only a small portion of photons generated in the LED active area can escape the device. There are two major loss mechanisms

[69] (1) losses due to re-absorption of the emitted photons and (2) losses resulted from the reflection at the semiconductor-air interface. PD-LED up-conversion devices normally have thin active LED region of several hundred nanometers, and low doping concentration in the range from 10^{16} to $10^{18}\,cm^{-3}$. The loss from re-absorption is negligible. The escape probability is therefore mainly limited by the photon reflection at the device surface.

The photon escape probability is very low for an ordinary planar LED. As imposed by the Snell's law, only those photons with incident angles smaller than the critical angle of total internal reflection, can escape from the LED surface [Fig. 12(a)] [68]. GaAs has a high refractive index of 3.7, leading to a small critical angle of 17%. As a result, the escape probability of photons from GaAs/AlGaAs LED is only about 2%. As shown previously, both the PD absorption efficiency and the LED internal efficiency have been improved to near 100%. Therefore, internal up-conversion quantum efficiencies close to 100% has been feasible. However, the external up-conversion quantum efficiency can be no higher than 2% using a simple planar GaAs/AlGaAs, mainly limited by the LED external efficiency.

While planar surface allows only a small portion of photons to escape, a spherical lens surface enables more to come out [Fig. 12(b)] [68]. For example, 20% of the light can be collected when the collection solid angle is 45°. We have fabricated a number of LEDs with

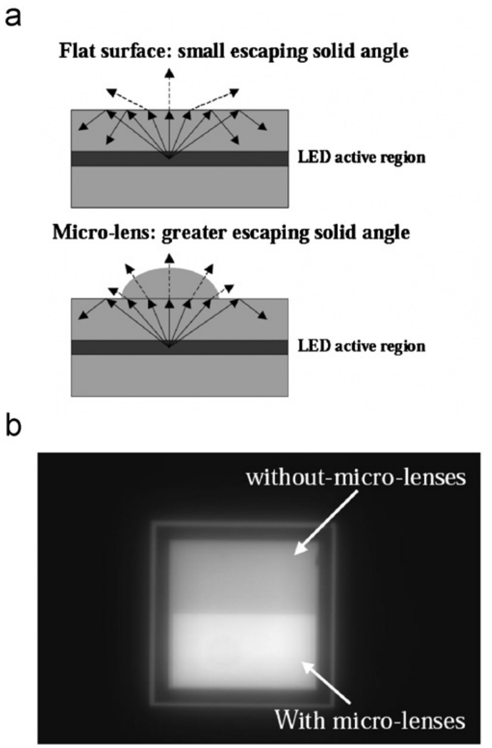

Fig. 12. (a) Schematic of photons escaping from LED surfaces with and without microlenses and (b) picture of a working GaAs/AlGaAs LED taking with a Si CCD (from Ref. [68]).

1.5 μm size near hemisphere shape microlens on top. The microlens was patterned by electron beam lithography and etched on top surface by dry etching. The external quantum efficiency of the LED was doubled [Fig. 12(b)]. So far the microlens had a poor shape and rough surface, and were far from optimized.

In addition to microlensed LEDs, several other schemes have been proposed to increase the external efficiencies [91–93], including resonant cavity LED structure, photon recycling, textured surface scattering, and 2D photonic crystal.

3.4. Other NIR up-conversion devices

3.4.1. Phototransistor-LED up-converters

For the cases discussed above, the PDs used are photodiodes. Considering a 1.5 μm photodiode, the idea responsivity is 1.12 A/W, when all incoming infrared photon are absorbed and every absorbed photon produces an electron–hole pair. On the LED side, the internal quantum efficiency has been improved to near 100%. Assuming 2% escape probability from the LED surface, the up-conversion efficiency is several percent W/W. As discussed above, LED external efficiency can be improved to about 20%, and accordingly the up-conversion device will be improved to about several tens percent W/W. To achieve even higher efficiencies, amplification structures may be used.

Optoelectronic devices with internal gain working in the NIR region include heterojunction phototransistors (HPTs) and avalanche photodiodes (APDs). A phototransistor is essentially a bipolar transistor with the base–collector junction as the light absorption layer. The electrons generated by photons in the base–collector junction are injected into the base, and this photodiode current is amplified by the transistor's current gain mechanism. HPTs can provide large gains at much lower bias than that required by APDs. In addition, they have lower noises. So far, NIR InGaAsP/InP, InGaAs/InP and AlGaAs/GaAs HPTs with gains of several hundred or even thousands of times have been demonstrated. Phototransistors have been used to substitute the photodiode, and much higher up-conversion efficiencies are obtained.

In 1981, Beneking et al. [53] constructed two monolithic wavelength up-converters separately composed of a phototransistor and a LED, both on AlGaAs/GaAs material system. With these devices, incident NIR photons were converted to visible photons of 775 and 680 nm. High up-conversion efficiencies of up to 1 and 10 W/W were obtained for the two devices. Note that the wavelength of light to be up-converted is restricted by the bandgap of GaAs material to short wavelength region (820 nm). The photons in this region can be directly detected by Si devices, making the device less attractive for practical NIR up-conversion imaging application. It does however point to a direction for future improvement.

In 2006, we built a 1.5–0.87 μm up-converter by integrating a GaAs InGaAs/InP HPT with a GaAs/AlGaAs LED via wafer fusion [77]. Fig. 13(a) shows the band diagram under 3 V bias, and a schematic of the device operation in the inset. Incoming 1.5 μm light is absorbed in the InGaAs base and collector layers, generating a primary electron photocurrent. The resulting holes flow to the base layer and generate an amplified photocurrent there. The HPT responsivity is 10 A/W for 2.2 mW/cm^2 input irradiance, and correspondingly the optical gain is 20. The LED quantum efficiency is 0.7% for the injection current density of 1.0 A/cm^2. With the integrated up-conversion device, an up-conversion efficiency of 0.1 W/W is reached [Fig. 13(b)]. Using a better LED structure

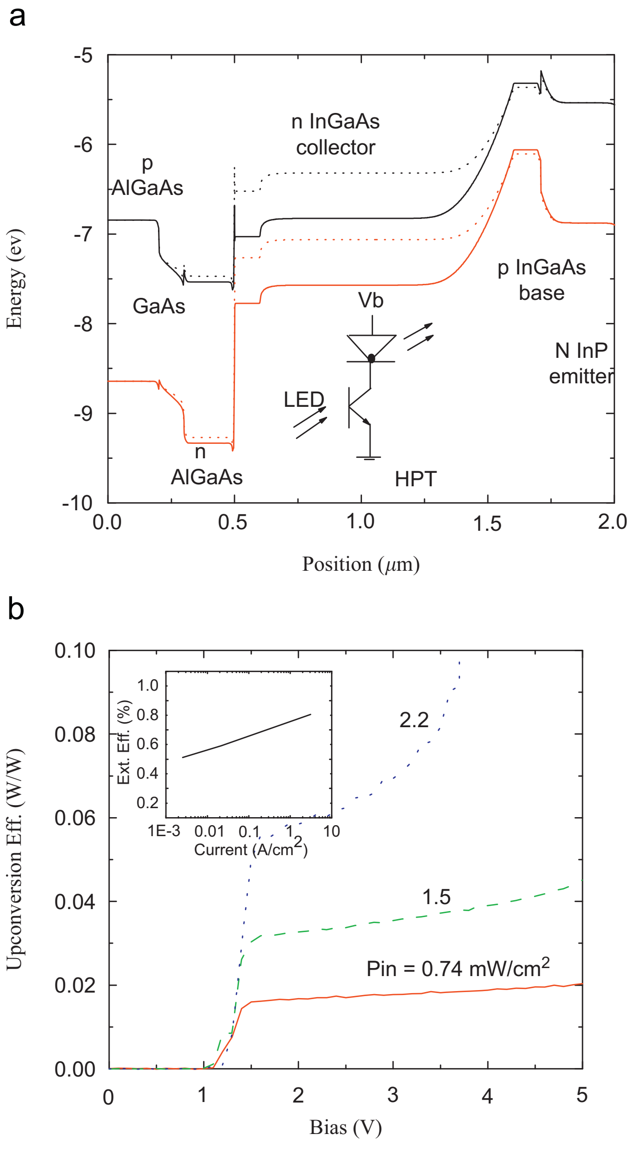

Fig. 13. Up-conversion devices with phototransistors: (a) band diagram scheme and (b) experimental results (from Ref. [77]).

(2% or higher quantum efficiency) and a HPT optimized for low input irradiance, up-conversion efficiency higher than unity can be expected.

3.4.2. Passive PD-LED up-converters

Another progress is the passive up-converter which does not need to be biased. This property is quite valuable for certain applications since it will largely reduce the size, complexity, and cost. To meet energy conversation law, infrared photons need to gain extra energy to convert to higher frequencies. For up-conversion devices those are biased, the extra energy is provided by the applied electric field. For passive up-converters, the general approach is to convert two or several infrared photons to one photon. In such cases, the sum energy of the absorbed photons exceeds the bandgap of LED.

In 2007, Zhao et al. [86] reported a two photon passive up-conversion device composed of three *p–n* junctions in stack, with the LED region sandwiched between two photodetection regions. The photodetection regions are *p–n* PDs using the interband transition of GaAs, and the LED active region is an $Al_{0.25}Ga_{0.75}As$ quantum well sandwiched between a *p–n* junction. Fig. 14(a) shows the band diagram scheme, and

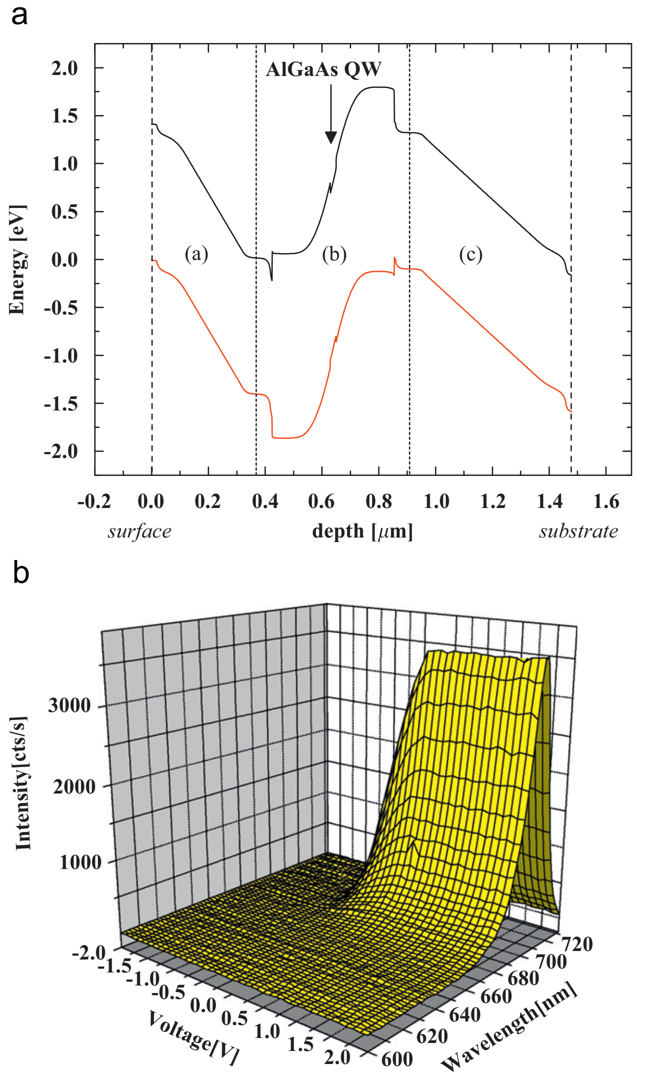

Fig. 14. Two-photon passive up-conversion device: (a) band diagram scheme and (b) experimental results (from Ref. [86]).

Fig. 14(b) shows the experimental results. This device up-converts 808 nm photons to 710 nm at RT. To suppress dark current, the LED region is oriented opposite to the two photodetection regions. This design turns out to be successful: the dark current is nearly zero even under high bias voltages, while obvious photocurrent and photocurrent induced luminescence are observed when the device illuminated.

3.4.3. Internal photoemission PD-LED up-converters

Though NIR PDs relying on interband transitions are more efficient, NIR up-converters relying on internal photoemission have been developed. Internal photoemission happens at either a Schottky barrier or the heterojunction of two semiconductor layers doped to different levels. In 2000, Sandhu et al. [62] demonstrated 1.5 μm to 808 nm up-conversion from an Au Schottky contact. The device was grown by depositing a semi-transparent Au layer on top of a GaAs/AlGaAs quantum well LED. The device works under low bias but very low temperatures (4 K).

In 2003, the operation temperature of internal photoemission NIR up-conversion device was increased to RT [67]. Fig. 15(a) schematically shows the energy band diagram of a metal–semiconductor Schottky diode in stack with a LED. The electrons are excited from the Fermi level to above the conduction band, and then moved to the quantum well. They recombine with holes in the quantum well and produce photons with higher energies. The device fabrication was started by growing a GaAs/AlGaAs quantum well LED on *p*-type GaAs substrate via MBE. Mesa devices were then processed using standard photolithographic techniques. After that, a semi-transparent Au layer was deposited on top of the LED. Fig. 15(b) shows the device electroluminescence (EL) under dark condition and 980 nm laser illumination. As indicated, the EL signal induced by 980 nm laser illumination is significantly larger than the EL signal under dark condition, though the photocurrent induced EL was taken under much lower bias. In 2006, an NIR up-conversion device using internal photoemission in an AlGaInP/GaInP quantum well heterostructure was demonstrated to emit visible light of 650 nm [78].

In addition to Schottky contact, a photoemission PD can be a heterojunction of two semiconductor layers, which are doped to different levels. Internal photoemission PDs are not as efficient as interband NIR PDs. Yet, up-conversion based on internal photoemission has two unique advantages. First, the response wavelength can be tuned within a wide wavelength range, via adjusting the height of Schottky contact or heterojunction. Until now, internal photoemission PDs for various wavelength ranges have been reported, from NIR to FIR, including the terahertz region. FIR up-conversion devices based on internal photoemission have been studied [79,83]. In contrast, the response wavelength of interband up-conversion devices is limited to the NIR region. Secondly, Schottky contact or internal photoemission heterojunction can be formed on various semiconductor layers. Thus, the output light can be tuned within a wide spectrum region as well. For example, we can envision an infrared to NIR up-converter by depositing a Schottky contact on top of GaAs/AlGaAs LED, and an infrared to visible up-converter by forming the internal photoemission structure on top of an AlGaInP/GaAsP LED.

3.4.4. Organic PD-LED up-converters

Besides inorganic devices, organic optoelectronic devices have been developing rapidly, and have been applied for NIR up-conversion. Organic optoelectronic devices are appropriate for

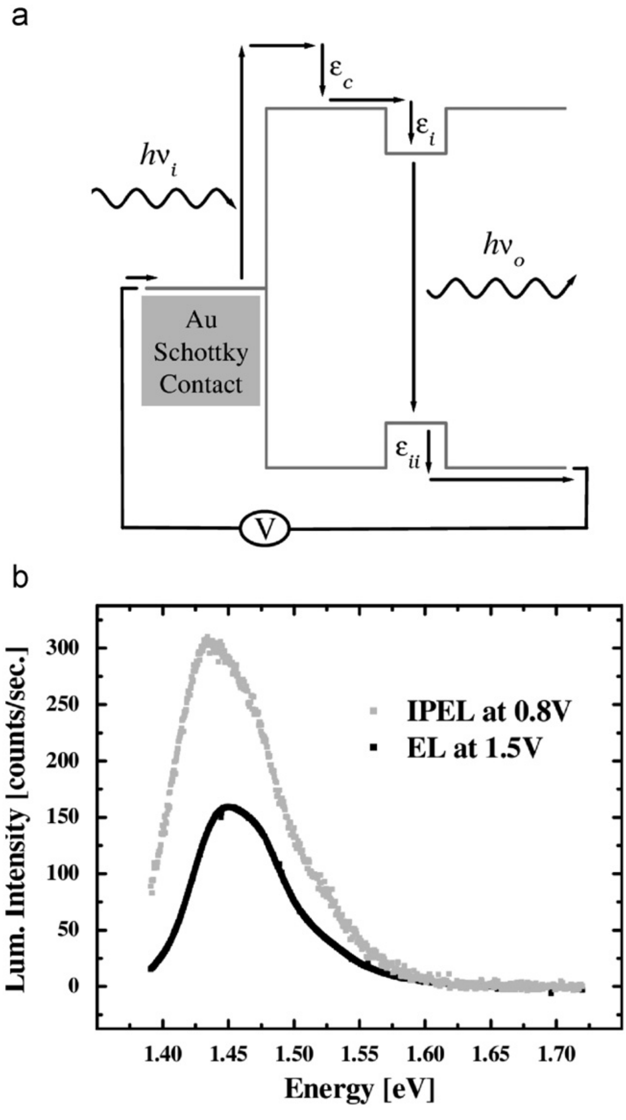

Fig. 15. Internal photoemission up-conversion device using a Schottky contact: (a) schematic of operation and (b) experimental results (from Ref. [67]).

NIR up-conversion due to two reasons. First, they can be flexibly disposed on various substrates with ease. One fundamental limitation of semiconductor optoelectronic devices is the need for lattice match between different layers. For example, InGaAs/InP PD has different lattice constant from GaAs/AlGaAs LED, making it impractical to grow them directly through epitaxial growth. In contrast to standard semiconductor devices, every organic optoelectronic molecular is a topologically perfect structure. The fabrication process can be simplified, and the cost can be reduced. Second, the emission wavelength of organic-LEDs (OLEDs) can be easily tuned to cover the NIR and visible region, while a LED based on GaAs or InP substrate limited to the red visible light and NIR.

The first organic PD-LED wavelength conversion device was demonstrated in 1990 by Hiramoto et al. [54]. via integrating an OLED with a photoresponsive amorphous silicon carbide (a-SiC:H) film. The emitter of LED was Tris (8-hydroxyquinoline) Aluminum complex (Alq_3) and the hole transport layer was *N*,*N*,*N*′,*N*′-tetrakis (mmethylphenyl)-1, 3-diaminobenzene (PDA). The excitation source is a 488 nm laser, and the output light peaked at 520 nm. One year later, they build a 633–520 nm up-conversion device with an up-conversion efficiency of 1%, using the same device structure [55]. In 1994, Katsume et al. demonstrated a full organic up-converter from 632.8 to 520 nm. Instead of a-SiC:H film, they used photoconductive organic pigment film (Me-PTC) as the photoresponsive layer. The Me-PTC film had with large photocurrent multiplication higher than 10,000 times, and correspondingly a high quantum efficiency of 40% was achieved [56]. However, these devices are not ideal for infrared imaging, since the light to be converted is visible. Moreover, they have to be operated at high bias voltages and under vacuum condition, and they do not respond fast enough, having response times in the second range. In 2002, a red to green up-conversion device working at low bias and ambient conditions was reported. It was

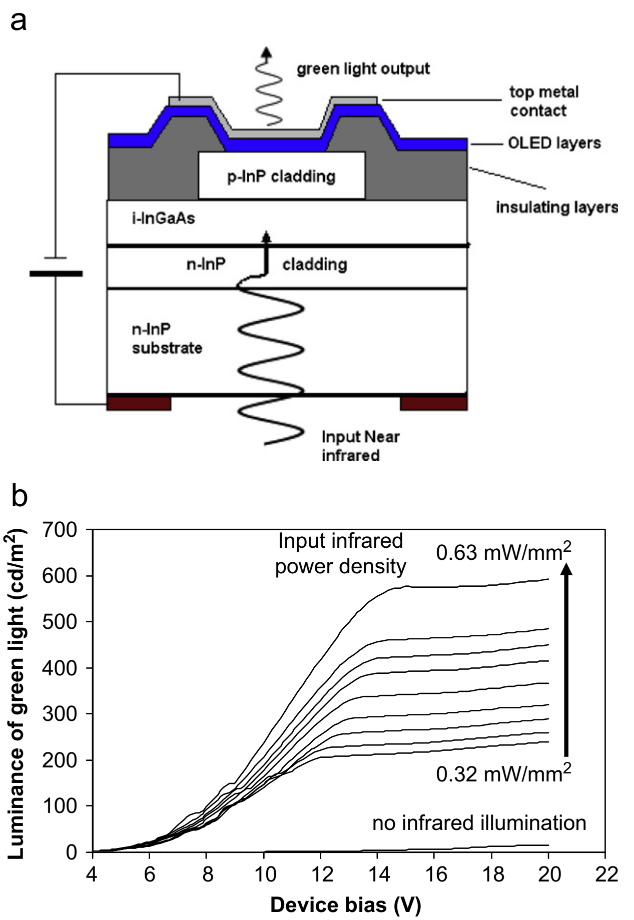

Fig. 16. Organic–inorganic up-conversion device: (a) device structure and (b) experimental results [80].

composed of a blue OLED with titanyl phthalocyanine as the infrared sensitive layer. The device was fast, with a response time of several hundreds of microseconds [63].

In 2007, the response wavelength of organic up-conversion device was extended to beyond 1 μm for the first time [80]. As shown in Fig. 16(a), the device was fabricated by direct tandem integration of an OLED with an InGaAs/InP *p–i–n* PD. An OLED device consists of a simple stack anode, a hole transport layer, a light-emitting layer, an electron transport layer, and a cathode layer. In the reported device, the *p*-doped InP layer of the *p–i–n* PD functions as the anode of the OLED. Fig. 16(b) shows the performance of the organic–inorganic up-conversion device. The green light luminance reaches up to 570 cd/m^2 under 14 V bias, when the device is illuminated by 0.63 mW/mm^2 1.5 μm NIR light. The illuminated to dark luminance ratio is more than 100 times.

The up-conversion efficiency was enhanced later by employing an embedded mirror in 2008, and the illuminated to dark luminance ratio was increased to 500 times [84]. By inserting a thin Au metal embedded mirror at the inorganic–organic interface, carriers are more effectively injected from the inorganic PD to the OLED. The NIR-induced green light luminance reached as high as 1580 cd/m^2 at a bias of 11.5 V with an input 1.5 μm NIR power density of 0.67 mW/mm^2.

3.5. NIR up-conversion imaging

While there has been much progress in NIR PD-LED up-conversion devices, the realization of a high performance infrared imaging is yet to come. In order to get good electric interconnections, the common region between the PD and LED should be heavily *p*-doped. In turn, this would result in significant carrier lateral diffusion. There is therefore a challenge in fabricating a NIR PD-LED pixelless imaging device: suppressing the lateral carrier diffusion in the common region while preserving effective electrical interconnection between the PD and LED.

NIR up-conversion imaging was not demonstrated until 2004, using a full InP-based up-converter grown by chemical beam epitaxy [71]. The photodetection structure was an $In_{0.53}Ga_{0.47}As$/InP *p–i–n* PD, with a 1-μm-thick undoped $In_{0.53}Ga_{0.47}As$ layer as the absorption region. The light-emitting structure was an $In_{0.93}Ga_{0.07}As_{0.16}P_{0.84}$/InP LED, with a 20-nm-thick $In_{0.93}Ga_{0.07}As_{0.16}P_{0.84}$ layer as the active layer. The layer structures and doping profiles were carefully designed, and a three-layer structure (undoped/doped/undoped) was adopted in the common region. Fig. 17(a) shows the band diagram and quasi-Fermi levels across the layer structure of the device under -3 V bias. There is a large separation between the electron/hole quasi-Fermi levels and the conduction/valence band edges, indicating that the lateral diffusion is significantly suppressed.

The LED output was negligible when the device is not illuminated. Under illumination of 1.47 μm laser, LED output centered at 1.02 μm was observed. Fig. 17(b) shows the RT emission spectra at different input power levels. The up-conversion efficiency of the device was low (about 1×10^{-4} W/W) due to the low internal and external efficiencies of the InGaAs/InP LED. Based on this device, proof-of-concept infrared imaging [shown in Fig. 17(c)] was demonstrated with the help of a Si CCD. The thin dark line at the top-right corner of the working device was a gold bonding wire. The image shows good contrast, and an estimated spatial resolution of around 50 μm is achieved.

As presented before, up-conversion devices fabricated by wafer fusing InP-based PD and GaAs-based LED have much higher quantum efficiencies. Wafer fused pixelless

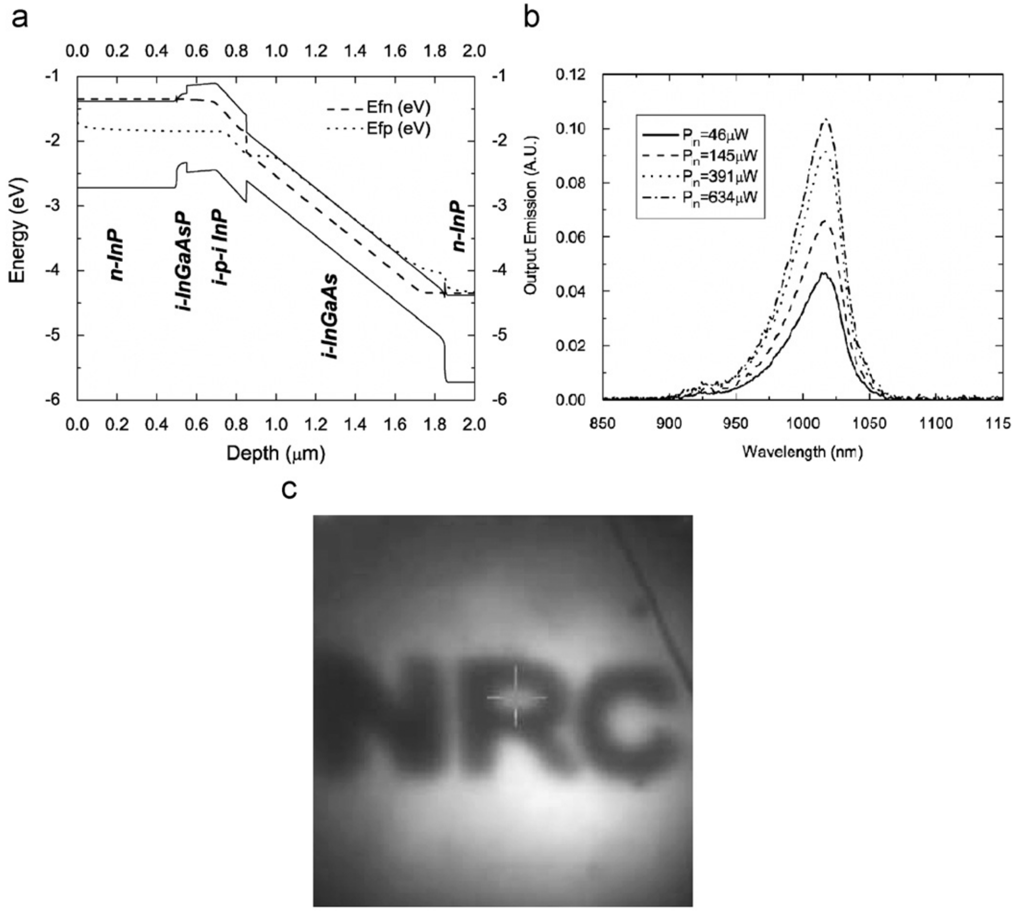

Fig. 17. Pixelless imaging using InP-based NIR PD-LED up-conversion device: (a) band diagram and quasi-Fermi levels, (b) RT output emission spectra at different input laser power levels, and (c) infrared image taken with up-conversion device and CCD (from Ref. [71]).

up-conversion imaging was demonstrated at RT in 2005 [72], as shown in Fig. 18. The device is composed of an InGaAs/InP *p–i–n* PD and a GaAs/AlGaAs LED, which were grown separately and wafer-bonded together. The InGaAs/InP *p–i–n* structure consists of a 1-μm-thick intrinsic $In_{0.53}Ga_{0.47}As$ absorption layer sandwiched between InP layers. The GaAs/AlGaAs LED structure consisted of a 30-nm-thick *p*-doped GaAs active layer sandwiched between AlGaAs barriers. First, the epitaxial surfaces are wafer fused together. After that the GaAs substrate of the LED is chemically removed and mesa devices are fabricated. The wafer fused device works as an *n–p–n* phototransistor. The common region indicated in Fig. 18(a) worked as a floating *p*-type base, the *n*-type InP layer served as the collector, and the *n*-type AlGaAs layer was the emitter. During operation, the photogenerated electrons produced in the InGaAs absorption layer moved to the *n*-InP layer, creating a primary photocurrent. Meanwhile, the photogenerated holes moved into the base and decreased the base-emitter potential, facilitating electrons to travel across the base to the collector, resulting in the amplified photocurrent.

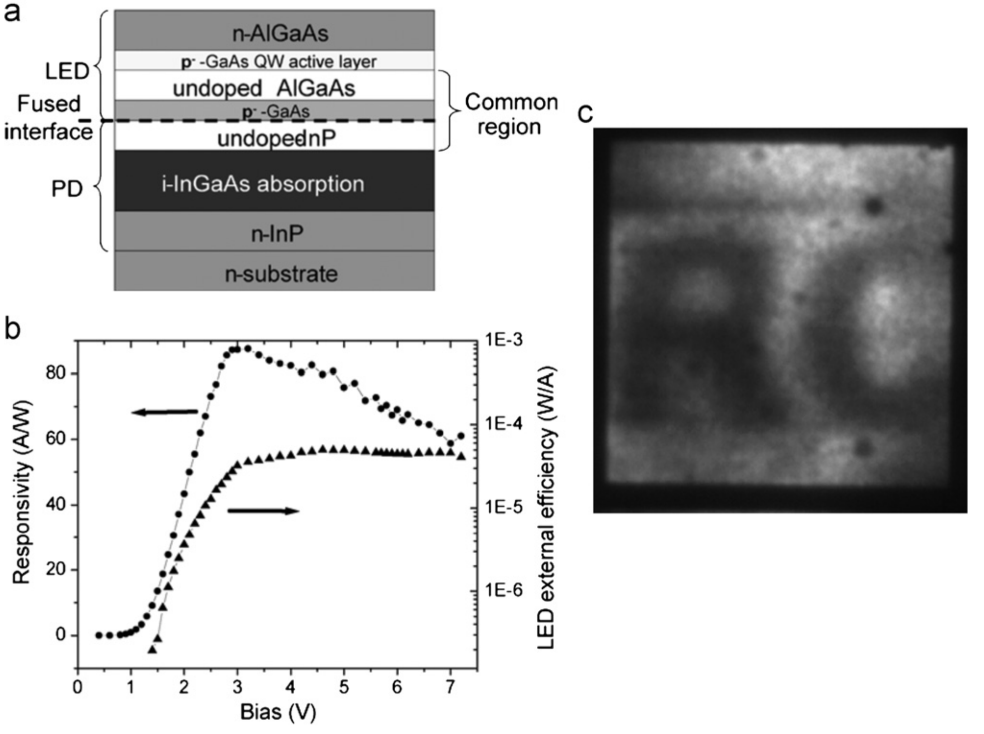

Fig. 18. Pixelless imaging using wafer fused NIR PD-LED up-conversion device: (a) device structure, (b) RT responsivity and light-emitting efficiency of the up-conversion device as a function of device bias, and (c) infrared image taken with up-conversion device and CCD (from Ref. [72]).

Fig. 18(b) shows RT responsivity and light-emitting efficiency of the up-conversion device as a function of device bias. The responsivity reached over 80 A/W at 3 V bias, corresponding to a photocurrent gain of more than 100 times. On the other hand, the LED external efficiency is very low (no higher than 5×10^{-5} W/A), less than 1% of the typical value. It should be noted that the poor LED efficiency is resulted from MBE growth, instead of wafer fusion process: The single LED devices based on the same MBE-grown wafer have very low external efficiencies as well. The internal quantum efficiency of the up-conversion device is 56%, and the external efficiency up-conversion efficiency is 0.1 W/W. Fig. 18(c) shows an example image captured using the wafer fused up-conversion device and a CCD camera. This study showed that wafer fusion provided a good electrical interconnection between the PD and LED, while largely suppressed the carrier diffusion at the interface.

The concept of PD-LED up-converters has also been successfully employed for MIR up-conversion imaging. In 1997, pixelless MIR up-conversion imaging based on a *p*-type QWIP-LED up-conversion device was demonstrated [21]. For the initial experiment to show the concept, image of a 1000-K hot object was captured, shown in Fig. 19(a). Thereafter, steady improvements were made [64,74,76]. Fig. 19 shows the progress of the research on QWIP-LED pixelless imaging, and a NETD of 60 mK was reached in 2004. The last picture [Fig. 19(f)] was taken with a QWIP-LED device having a *n*-type GaAs/AlGaAs QWIP peaked at a wavelength of 9 μm and a GaAs LED emitting at

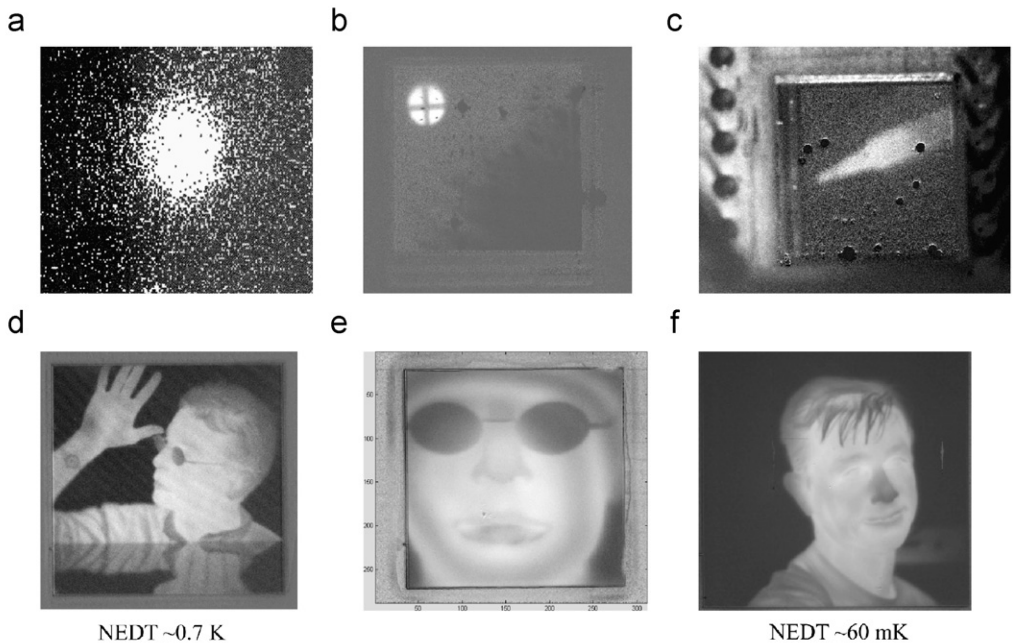

Fig. 19. Development of QWIP-LED pixelless imaging. (a) Feb. 1997, (b) Aug. 1999, (c) Sept. 1999, (d) Jan. 2001, (e) Jul. 2004 and (f) Aug. 2004.

820 nm. The experiment was done with the device operating at 63 K. The QWIP spectral peak responsivity was 0.3 A/W and the LED internal efficiency was 54%, which resulted in a power conversion efficiency of 0.24 W/W. The full details of the experiment as well as theoretical model and analyses were given in Refs. [64,74]. It should be noted that the imaging quality was completely limited by the CCD full-well capacity ($\sim 3 \times 10^5$ in this case). If we have had a CCD with 10 times larger full-well capacity, we would have obtained an NEDT of better than 20 mK. As a general comment, though the potential of QWIP-LED pixelless imaging has been demonstrated in our lab, to fully develop it into a technology and enter the commercial market, two things are still needed: (1) a manufacturable QWIP-LED fabrication process with reasonable yield, and (2) a packaging process to intimately integrate QWIP-LED and CCD with high external and transfer efficiencies. The most critical obstacle that must be overcome is producing nearly defect-free large-area epitaxial materials though limited number of defects may be removed after growth, for example for laser ablation [64,74].

4. Conclusion

In this paper, we present a systematic review on infrared up-conversion, especially NIR semiconductor up-conversion devices for the purpose of infrared imaging. Various up-conversion techniques relying on different mechanisms are discussed, with their own advantages and drawbacks.

One interesting application of photon up-conversion is pixelless infrared imaging. The current standard way for infrared imaging is FPAs, which relies on a complicated fabrication process and is therefore costly. One alternative approach of infrared imaging is to up-convert the infrared photons to higher frequencies and then detect them with mature Si devices. Among all types of up-conversion techniques, PD-LED up-conversion is the most appropriate for this purpose, due to the unique characteristics including simplicity and compactness, low cost, wide response range, good flexibility, and high up-conversion efficiency.

A PD-LED up-converter is typically composed of two major parts, a PD and a LED. Incident infrared photons are absorbed by the PD, resulting in a photocurrent that drives the LED to emit photons with a shorter wavelength. So far, PD-LED up-conversion photodetection and imaging for different wavelength ranges have been investigated, from NIR to terahertz. Depending on the response region, various PD structures relying on interband, intersubband transitions or internal photoemissions have been used, while the light-emitting part is an organic or inorganic LED.

NIR up-conversion devices with high quantum efficiencies have been demonstrated. PDs relying on interband transitions routinely have near 100% absorption efficiencies, and the LED internal efficiency have also been improved to near 100%. Accordingly, internal up-conversion quantum efficiencies close to 100% has been approached. However, the external up-conversion efficiency is still low (several percent), mainly limited by the small photon escape probability from the LED surface. Further studies are under way to address this problem. Meanwhile, up-conversion device with gain mechanisms have been demonstrated, capable of high up-conversion efficiencies close to or larger than unity. In addition to NIR up-conversion devices based on interband transitions, several special types of NIR PD-LED up-conversion devices have been demonstrated, including photoemission up-converters, organic up-converters, and two photon passive up-converters. They have their own characteristics and advantages.

Using up-conversion devices in combination of Si CCDs, pixelless infrared imaging has been demonstrated. There is a challenge in fabricating a NIR PD-LED pixelless imaging device: suppressing the lateral carrier diffusion in the common region while preserving effective electrical interconnection between the PD and LED. We have overcome this problem and demonstrated pixelless infrared imaging in both NIR and MIR wavelength range. Further investigations are called for to improve the quantum efficiency and minimize the crosstalk, to make pixelless up-conversion imaging a practical technique.

Acknowledgments

This work was supported in part by the National Major Basic Research Projects (2011CB925603 and 2010CB933702), Shanghai Municipal Major Basic Research Project (09DJ1400102), and the Natural Science Foundation of China (10734020).

References

[1] B.R. Reddy, P. Venkateswarlu, Appl. Phys. Lett. 64 (1994) 1327–1329.
[2] E.B. Mejia, A.N. Starodumov, Y.O. Barmenkov, Appl. Phys. Lett. 74 (1999) 1540–1542.
[3] F. Auzel, Chem. Rev. 104 (2003) 139–174.
[4] G.K. Samanta, M. Ebrahim-Zadeh, Opt. Lett. 33 (2008) 1228–1230.
[5] E. Downing, L. Hesselink, J. Ralston, R. Macfarlane, Science 273 (1997) 1185–1189.
[6] G.S. Maciel, A. Biswas, R. Kapoor, P.N. Prasad, Appl. Phys. Lett. 76 (2000) 1978–1980.

[7] T.R. Hinklin, S.C. Rand, R.M. Laine, Adv. Mater. 20 (2008) 1270–1273.
[8] T. Trupke, M.A. Green, P. Wurfel, J. Appl. Phys. 92 (2002) 4117–4122.
[9] B.S. Richards, A. Shalav, IEEE Trans. Electron. Dev. 54 (2007) 2679–2684.
[10] A. Shalav, B.S. Richards, M.A. Green, Sol. Energy Mater. Sol. Cells 91 (2007) 829–842.
[11] T. Kushida, J.E. Geusic, Phys. Rev. Lett. 21 (1968) 1172–1175.
[12] M.H. Anderson, J.R. Ensher, M.R. Matthews, C.E. Wieman, E.A. Cornell, Science 269 (1995) 198–201.
[13] C.E. Mungan, M.I. Buchwald, B.C. Edwards, R.I. Epstein, T.R. Gosnell, Phys. Rev. Lett. 78 (1997) 1030–1033.
[14] D.V. Seletskiy, S.D. Melgaard, S. Bigotta, A. Di Lieto, M. Tonelli, M. Sheik-Bahae, Nat. Photonics 4 (2010) 161–164.
[15] M.A. Albota, F.N.C. Wong, Opt. Lett. 29 (2004) 1449–1451.
[16] A.P. Vandevender, P.G. Kwiat, J. Mod. Opt. 51 (2004) 1433–1445.
[17] E. Diamanti, H. Takesue, T. Honjo, K. Inoue, Y. Yamamoto, Phys. Rev. A 72 (2005) 052311.
[18] C. Langrock, E. Diamanti, R.V. Roussev, Y. Yamamoto, M.M. Fejer, H. Takesue, Opt. Lett. 30 (2005) 1725–1727.
[19] R.H. Hadfield, Nat. Photonics 3 (2009) 696–705.
[20] R.F. Lucy, Appl. Opt. 11 (1972) 1329–1336.
[21] H.C. Liu, L.B. Allard, M. Buchanan, Z.R. Wasilewski, Electron. Lett. 33 (1997) 379–380.
[22] E. Dupont, H.C. Liu, M. Buchanan, Z.R. Wasilewski, D. St-Germain, P. Chevrette, Appl. Phys. Lett. 75 (1999) 563–565.
[23] A. Rogalski, Prog. Quantum Electron. 27 (2003) 59–210.
[24] S.D. Gunapala, S.V. Bandara, J.K. Liu, C.J. Hill, S.B. Rafol, J.M. Mumolo, J.T. Trinh, M.Z. Tidrow, P.D. LeVan, Semicond. Sci. Technol. 20 (2005) 473–480.
[25] S. Krishna, D. Forman, S. Annamalai, P. Dowd, P. Varangis, T. Tumolillo, A. Gray, J. Zilko, K. Sun, M.G. Liu, J. Campbell, D. Carothers, Appl. Phys. Lett. 86 (2005) 193501.
[26] A. Rogalski, Rep. Prog. Phys. 68 (2005) 2267.
[27] A. Rogalski, J. Antoszewski, L. Faraone, J. Appl. Phys. 105 (2009) 091101.
[28] G. Riedl, M. Assel, A. Fendt, W. Hetzer, E. Keller, F. Kilger, T. Kuligk, L. Popp, R. Proels, N. Schweyer, Proc. SPIE 4369 (2001) 201–209.
[29] M.Z. Tidrow, W.R. Dyer, Infrared Phys. Technol. 42 (2001) 333–336.
[30] M.R. Clark, D.M. McCann, M.C. Forde, NDT&E. Int. 36 (2003) 265–275.
[31] D.J. Hawrysz, E.M. Sevick-Muraca, Neoplasia 2 (2000) 388–417.
[32] J.F. Head, F. Wang, C.A. Lipari, R.L. Elliott, IEEE Eng. Med. Biol. Mag. 19 (2000) 52–57.
[33] R.M. El-Agmy, Laser Phys. 18 (2008) 803–806.
[34] M.J. Khan, J.C. Chen, S. Kaushik, Opt. Lett. 33 (2008) 2725–2727.
[35] C.M. Lai, I.N. Hu, Y.Y. Lai, Z.X. Huang, L.H. Peng, A. Boudrioua, A.H. Kung, Opt. Lett. 35 (2010) 160–162.
[36] A.N. Titkov, G.N. Iluridze, I.F. Mironov, V.A. Cheban, Sov. Phys. Semicond. 20 (1986) 14.
[37] M. Potemski, R. Stepniewski, J.C. Maan, G. Martinez, P. Wyder, B. Etienne, Phys. Rev. Lett. 66 (1991) 2239–2242.
[38] W. Seidel, A. Titkov, J.P. André, P. Voisin, M. Voos, Phys. Rev. Lett. 73 (1994) 2356–2359.
[39] F.A.J.M. Driessen, H.M. Cheong, A. Mascarenhas, S.K. Deb, P.R. Hageman, G.J. Bauhuis, L.J. Giling, Phys. Rev. B 54 (1996) R5263–R5266.
[40] F.A.J.M. Driessen, H.M. Cheong, Appl. Phys. Lett. 70 (1997) 1630.
[41] E.K. Lee, D. Lockwood, J.M. Baribeau, A. Bratkovsky, T. Kamins, L. Tsybeskov, Phys. Rev. B 79 (2009) 233307.
[42] A. Tomita, J. Shah, J.E. Cunningham, S.M. Goodnick, P. Lugli, S.L. Chuang, Phys. Rev. B 48 (1993) 5708–5711.
[43] R. Hellmann, A. Euteneuer, S.G. Hense, J. Feldmann, P. Thomas, E.O. Gobel, D.R. Yakovlev, A. Waag, G. Landwehr, Phys. Rev. B 51 (1995) 18053–18056.
[44] Z.P. Su, K.L. Teo, P.Y. Yu, K. Uchida, Solid State Commun. 99 (1996) 933–936.
[45] T. Nishikawa, M. Yokota, S. Nakamura, Y. Kadoya, M. Yamanishi, I. Ogura, IEEE Photonics Technol. Lett. 9 (1997) 179–181.
[46] J. Zeman, G. Martinez, P.Y. Yu, K. Uchida, Phys. Rev. B 55 (1997) R13428–R13431.
[47] P.P. Paskov, P.O. Holtz, B. Monemar, J.M. Garcia, W.V. Schoenfeld, P.M. Petroff, Appl. Phys. Lett. 77 (2000) 812–814.

[48] T. Kobayashi, H. Tomoda, A.D. Prins, Y. Homma, K. Uchida, J. Nakahara, Phys. Status Solidi B 235 (2003) 277–281.
[49] S.J. Xu, Q. Li, J.R. Dong, S.J. Chua, Appl. Phys. Lett. 84 (2004) 2280–2282.
[50] P.W. Kruse, F.C. Pribble, R.G. Schulze, J. Appl. Phys. 38 (1967) 1718–1720.
[51] R.J. Phelan Jr., Proc. IEEE 55 (1967) 1501–1502.
[52] H. Beneking, H. Schul, G. Mischel, G. Schul, A. Gattung, Electron. Lett. 10 (1974) 346–347.
[53] H. Beneking, N. Grote, M.N. Svilans, IEEE Trans. Electron Dev. 28 (1981) 404–407.
[54] M. Hiramoto, T. Miyao, M. Yokoyama, Appl. Phys. Lett. 57 (1990) 1625–1627.
[55] M. Hiramoto, K. Yoshimura, T. Miyao, M. Yokoyama, Appl. Phys. Lett. 58 (1991) 1146–1148.
[56] T. Katsume, M. Hiramoto, M. Yokoyama, Appl. Phys. Lett. 64 (1994) 2546–2548.
[57] H.C. Liu, J. Li, Z.R. Wasilewski, M. Buchanan, Electron. Lett. 31 (1995) 832–833.
[58] H.C. Liu, US Patent, No. 5567955, Issue date Oct. 22, 1996.
[59] L.B. Allard, H.C. Liu, M. Buchanan, Z.R. Wasilewski, Appl. Phys. Lett. 70 (1997) 2784–2786.
[60] H.C. Liu, US Patent, No. 6028323, Issue date Feb. 22, 2000.
[61] H.C. Liu, M. Gao, P.J. Poole, Electron. Lett. 36 (2000) 1300–1301.
[62] J.S. Sandhu, A.P. Heberle, B.W. Alphenaar, J.R.A. Cleaver, Appl. Phys. Lett. 76 (2000) 1507–1509.
[63] M. Chikamatsu, Y. Ichino, N. Takada, M. Yoshida, T. Kamata, K. Yase, Appl. Phys. Lett. 81 (2002) 769–771.
[64] E. Dupont, M. Byloos, M. Gao, M. Buchanan, C.Y. Song, Z.R. Wasilewski, H.C. Liu, IEEE Photonics Technol. Lett. 14 (2002) 182–184.
[65] D. Ban, H. Luo, H.C. Liu, A.J. SpringThorpe, R. Glew, Z.R. Wasilewski, M. Buchanan, Electron. Lett. 39 (2003) 1145–1147.
[66] M. Buchanan, M. Byloos, S. Chiu, E. Dupont, M. Gao, H.C. Liu, C.Y. Song, US Patent, No. 6576490, Issue date June 10, 2003.
[67] K.J. Russell, I. Appelbaum, H. Temkin, C.H. Perry, V. Narayanamurti, M.P. Hanson, A.C. Gossard, Appl. Phys. Lett. 82 (2003) 2960–2962.
[68] D. Ban, Proc. SPIE 5543 (2004) 47–55.
[69] D. Ban, H. Luo, H.C. Liu, Z.R. Wasilewski, A.J. SpringThorpe, R. Glew, M. Buchanan, J. Appl. Phys. 96 (2004) 5243–5248.
[70] M. Buchanan, M. Byloos, S. Chiu, E. Dupont, M. Gao, H.C. Liu, C.Y. Song, US Patent, No. 6750072, Issue date June 15, 2004.
[71] H. Luo, D. Ban, H.C. Liu, P.J. Poole, M. Buchanan, IEEE Electron. Dev. Lett. 25 (2004) 129–131.
[72] D. Ban, H. Luo, H.C. Liu, Z.R. Wasilewski, M. Buchanan, IEEE Photonics Technol. Lett. 17 (2005) 1477–1479.
[73] D. Ban, H. Luo, H.C. Liu, Z.R. Wasilewski, Y. Paltiel, A. Raizman, A. Sher, Appl. Phys. Lett. 86 (2005) 201103.
[74] E. Dupont, M. Byloos, T. Oogarah, M. Buchanan, H.C. Liu, Infrared Phys. Technol. 47 (2005) 132–143.
[75] H.C. Liu, D. Ban, H. Luo, US Patent, No. 7079307, Issue date July 18, 2006.
[76] H. Schneider, H.C. Liu, Quantum Well Infrared Photodetectors—Physics and Applications, 126, Springer, 2006.
[77] H. Luo, D. Ban, H.C. Liu, Z.R. Wasilewski, M. Buchanan, Appl. Phys. Lett. 88 (2006) 073501.
[78] M.R. Olson, K.J. Russell, V. Narayanamurti, J.M. Olson, I. Appelbaum, Appl. Phys. Lett. 88 (2006) 161108.
[79] L.K. Wu, W.Z. Shen, J. Appl. Phys. 100 (2006) 044508.
[80] D. Ban, S. Han, Z.H. Lu, T. Oogarah, A.J. SpringThorpe, H.C. Liu, IEEE Trans. Electron Dev. 54 (2007) 1645–1650.
[81] D. Ban, S. Han, Z.H. Lu, T. Oogarah, A.J. SpringThorpe, H.C. Liu, Appl. Phys. Lett. 90 (2007) 093108.
[82] J.S. Lu, Y. Zheng, Z.J. Chen, L.X. Xiao, Q.H. Gong, Appl. Phys. Lett. 91 (2007) 201107.
[83] L.K. Wu, W.Z. Shen, IEEE J. Quantum Electron. 43 (2007) 411–418.
[84] J. Chen, D. Ban, X.D. Feng, Z.H. Lu, S. Fathololoumi, A.J. SpringThorpe, H.C. Liu, J. Appl. Phys. 103 (2008) 103112.
[85] Y. Yang, W.Z. Shen, H.C. Liu, S.R. Laframboise, S. Wicaksono, S.F. Yoon, K.H. Tan, Appl. Phys. Lett. 94 (2009) 093504.
[86] L. Zhao, P. Thompson, N.N. Faleev, D.W. Prather, I. Appelbaum, Appl. Phys. Lett. 90 (2007) 121132.
[87] J.B. Heroux, X. Yang, W.I. Wang, Appl. Phys. Lett. 75 (1999) 2716–2718.
[88] H. Luo, J.A. Gupta, H.C. Liu, Appl. Phys. Lett. 86 (2005) 211121.
[89] J.S. Ng, W.M. Soong, M.J. Steer, M. Hopkinson, J.P.R. David, J. Chamings, S.J. Sweeney, A.R. Adams, J. Appl. Phys. 101 (2007) 064506.

[90] A. Black, A.R. Hawkins, N.M. Margalit, D.I. Babic, A.L. Holmes, Y.L. Chang, P. Abraham, J.E. Bowers, E.L. Hu, IEEE J. Sel. Top. Quantum Electron. 3 (1997) 943–951.
[91] I. Schnitzer, E. Yablonovitch, C. Caneau, T.J. Gmitter, Appl. Phys. Lett. 62 (1993) 131–133.
[92] H. De Neve, J. Blondelle, R. Baets, P. Demeester, P. Van Daele, G. Borghs, IEEE Photonics Technol. Lett. 7 (1995) 287–289.
[93] H. Benisty, H. De Neve, C. Weisbuch, IEEE J. Quantum Electron. 34 (1998) 1612–1631.